Power and Particle Exhaust in an ST-FNSF*

J.M. Canik[1], T.K. Gray[1], R. Maingi[2], J.E. Menard[2]

[1]Oak Ridge National Laboratory, Oak Ridge, TN, USA
[2]Princeton Plasma Physics Laboratory, Princeton, NJ USA
Corresponding author e-mail: canikjm@ornl.gov.

***Abstract*— A spherical tokamak (ST) configuration is favorable for a Fusion Nuclear Science Facility (FNSF), due to its small size and relatively low cost. However, the compactness of the ST also exacerbates the power and particle handling problems anticipated in next-step devices, since local fluxes are higher and less space is available for optimizing plasma-facing components. Here we present an analysis of the power and particle handling requirements of a candidate ST-FNSF, based on 0-D exhaust projections as well as 2-D edge plasma modeling using the SOLPS code. These show that, for reasonable assumptions on cross-field transport, operating points can be identified that are consistent with both core plasma operation and power and particle exhaust requirements.**

Keywords—divertor; FNSF;

I. INTRODUCTION

The small size and related low cost of the spherical tokamak (ST) make it attractive as the basis for a Fusion Nuclear Science Facility (FNSF) [1]. Recent design studies have explored the feasibility of realizing such an ST-FNSF [2]. While consistent core plasma physics scenarios have been found compatible with such a device, the compactness of the ST also leads to potential difficulties with power and particle handling. Due to the smaller plasma-wetted area, high heat fluxes are expected, and relatively short field line connection lengths make conventional radiative dispersal methods more challenging [3]. Further, the lack of space near the plasma core limits the possible size of internal components, making highly shape-optimized divertor structures and pumping systems difficult to implement. Here we present an analysis of the power and particle handling requirements of a candidate ST-FNSF, with the goal of identifying, if possible, divertor configurations and core operating scenarios that are compatible with long-pulse divertor operations. Further, pumping in simplified geometries is analyzed for its potential to provide the needed particle control without compromising the device compactness. This analysis is based on 0-D projections of the power and particle exhaust requirements and capabilities, as well as 2-D edge plasma modeling to more precisely define viable scenarios.

II. POWER EXHAUST CALCULATIONS

A primary challenge to the feasibility of next-step devices such as the ST-FNSF is exhausting the very high heat fluxes that are anticipated in the divertor. While projections of the divertor heat flux have historically shown wide variations, recent joint experiments have been carried out across a number of tokamak devices in order to improve the data set used for these projections [4-6]. These have yielded scalings for the width of the power-carrying channel in the scrape-off layer (SOL), λ_q, that are rather pessimistic. For example, the projected SOL width for ST-FNSF based on a recent purely empirical scaling [7] yields λ_q=2.6 mm, while another projection using a drift-based theoretical model [8] yields 1.3 mm. Assuming that the magnetic field has a grazing angle of incidence on the divertor surface of 1 degree (either through

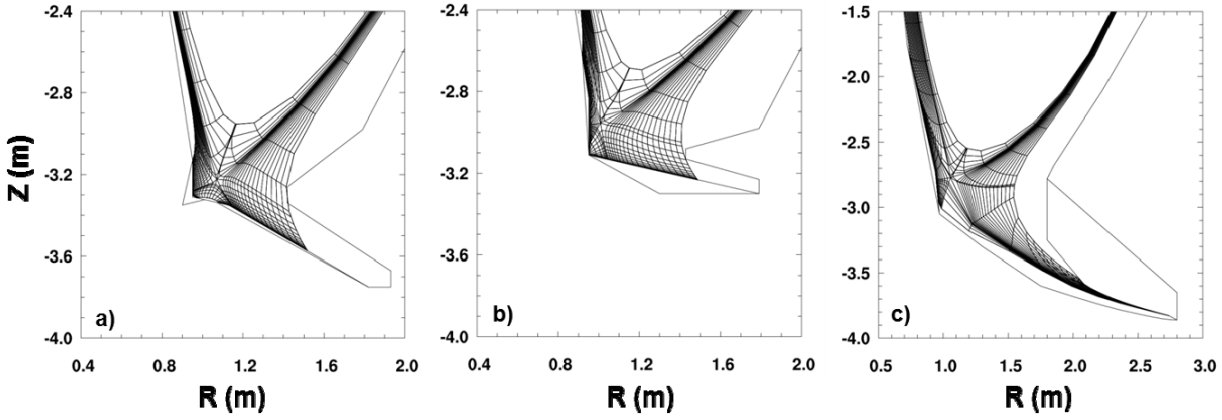

Fig. 1: Divertor configurations and computational grids for a a) Standard divertor, b) Snowflake, and c) Super-X

*This work supported by the US DOE Contracts DE-AC05-00OR22725 and DE-AC02-09CH11466

978-1-4799-0171-5/13/$31.00 ©2013 IEEE

magnetic flux expansion or by poloidal inclination of the target), these yield peak heat fluxes in excess of 50 MW/m^2. Since conventional carbon-based divertor technologies are limited to < 10 MWm^2 in steady-state, and at present W-based systems to even less (~5-8 MW/m^2) [9], the large natural heat flux in ST-FNSF must be dispersed via, e.g., strong radiation for the divertor scenario to be viable. In addition to a sufficiently low heat flux, the divertor of an ST-FNSF must also operate at low electron temperature T_e in order to minimize net erosion and ensure long PFC lifetime. Estimates of the acceptable temperature range indicate that the divertor electron temperature must be less than ~10 eV [10] (although T_e above 2 eV may also be necessary to ensure high core plasma confinement).

To examine the prospects for achieving heat fluxes on the order of 5 MW/m^2 and temperatures of 2-10 eV, simulations of the ST-FNSF SOL and divertor have been carried out using the SOLPS code [11]. This code uses a 2D fluid treatment of the plasma transport (using the B2 code [12]), coupled to a Monte-Carlo neutral transport calculation of the recycled neutrals (using EIRENE [13]). Transport is assumed to be classical parallel to the magnetic field (with kinetic corrections), and cross-field transport is governed by user-specified anomalous transport coefficients. Since at present a physics-based prediction of these coefficients is not readily available, they have instead been chosen to produce a SOL width that is in the range predicted by the multi-machine scaling experiments. The power flowing to the plasma edge is input as 50 MW in the simulations; i.e., it is assumed that ~55% of the 110 MW total plasma heating power is dissipated by radiation in the core. The assumed edge power is still well above the L-H transition threshold [14], estimated to be 15-30 MW. The density at the core-most grid cell is set as a boundary condition and is used in the density scans to be described below. Radiation from nitrogen seeding at a fixed fraction of 2% is included.

Three divertor configurations have been modeled: a Standard divertor, a Snowflake divertor [15], and a long-legged Super-X-like [16] configuration. These are illustrated in Figure 1, which shows the SOLPS grid along with the vacuum boundary. A tentative pumping duct is also shown for the Standard and Snowflake cases, although in these particular simulations pumping is not included. The Standard and Snowflake configurations differ primarily in the poloidal flux expansion, which is significantly larger for the Snowflake; the geometric spreading of the heat flux is comparable, however, since the poloidal inclination is increased in the Standard configurations, such that the total field line angle of incidence is 1^o for both cases. The Snowflake does show an increased connection length, although the magnitude of the increase for this particular equilibrium (~20%) is modest compared to that achieved in other Snowflake studies. Due to the larger major radius of the strike point in the Super-X configuration (2.6 vs 1.1 m), the magnetic field strength and hence the parallel heat flux are reduced, giving further geometric heat flux reductions than are possible with the Standard or Snowflake divertors.

The transport coefficients used for the initial set of calculations are D=0.3 and $\chi_e=\chi_i=1.0$ m^2/s; these are the standard transport assumptions made for predictive ITER divertor modeling [17]. The SOL width in the simulations is measured by taking the full-width half-max of the radial profile of the parallel heat flux at the poloidal location of the X-point. This location is chosen since it is where the heat flux is largest: all of the power has crossed from the core into the SOL, but volumetric losses in the divertor have not yet dissipated much power. The SOL widths based on this method are shown in Figure 2, where a density scan has been performed while keeping the transport coefficients constant. At moderate density, this yields a SOL width in the range of λ_q=2-2.5 mm for the Standard and Snowflake configurations (note that at the highest densities for these configurations, significant radiation occurs in the far SOL above the X-point, artificially reducing the SOL width). This is consistent with the empirical projection given above. For the Super-X, a

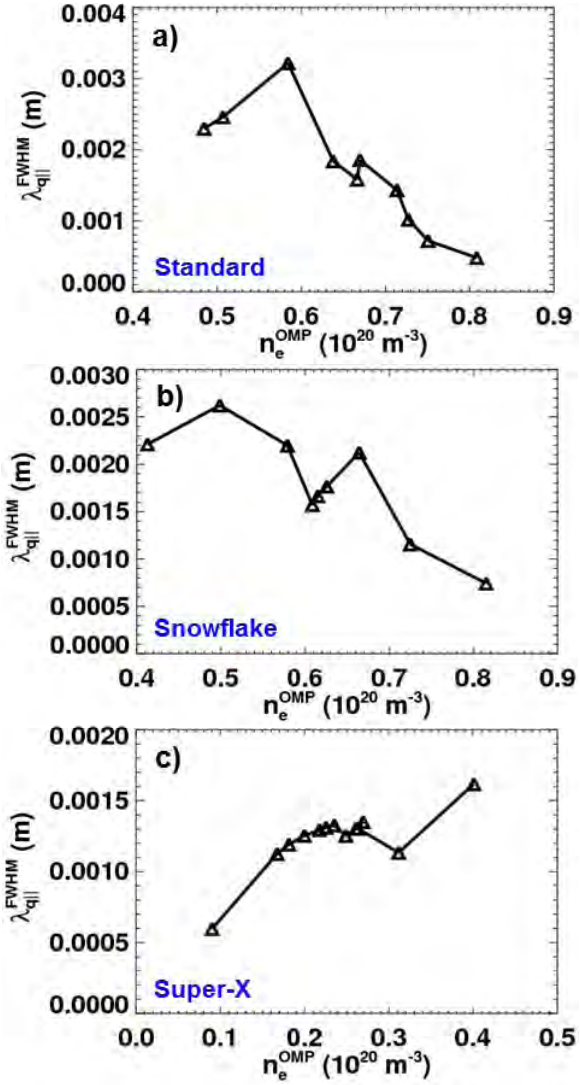

Fig. 2: SOL width measured at the poloidal location of the X-point over a range of core densities for the a) Standard, b) Snowflake, and c) Super-X divertor configurations

heat flux above this value. The Super-X shows a much

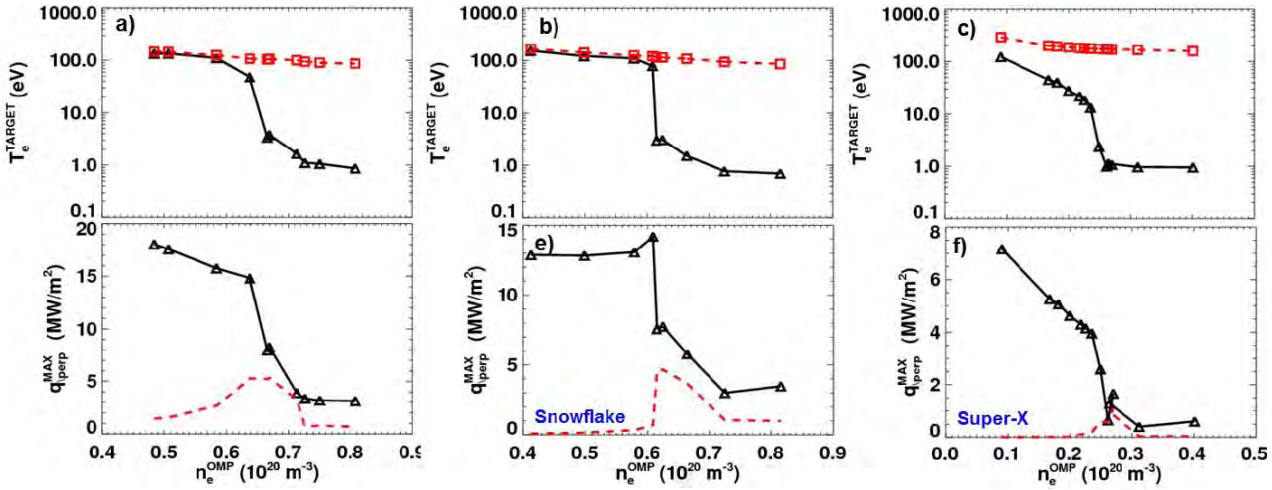

Fig. 3: Dependence on midplane density of a-c divertor temperature and d-f heat flux for a,c) Standard, b,d) Snowflake, and c,e) Super-X divertor configurations. Upstream temperature and radiant component of power load are indicated by dashed red curves.

narrower SOL is found, with λ_q~1.2 mm. This is due to the higher upstream SOL temperature in this configuration, which results in much higher parallel transport rates and hence a narrowing of the heat flux channel. However, in this configuration significant broadening of the power channel occurs between the X-point and target due to the very extended divertor leg, which is not reflected in the width calculation presented here.

The core density scan performed in the simulations allows the mapping out of divertor operating space so that, for this value of the SOL width, conditions for achieving acceptable divertor parameters can be identified. The results are shown in Figure 3, where the divertor heat flux and T_e, are plotted vs. the density at the outer midplane. The heat flux is the maximum value along the outer divertor, while the plasma parameters are shown for the flux tube located 0.1 mm outside the separatrix at the midplane in the simulation. The simulations show first of all that an acceptable divertor scenario can be created for all three divertor configurations, for the assumed level of cross-field transport. This requires operation at relatively high upstream densities, where the heat flux is reduced to < 5MW/m^2 by radiation, and the temperature is reduced below ~10 eV. At the highest densities the simulations are near or past the onset of full divertor detachment, which is likely inconsistent with good core confinement. To avoid this, further optimization of, e.g., divertor gas puff or PFC geometry can be performed to induce partial detachment only near the strike point where the heat fluxes are highest; this will be tested in future simulations. The required density for reaching low T_e and heat flux varies with configuration, with the standard divertor requiring the highest density of ~6.5×10^{19} m^{-3}. However, this particular ST-FNSF scenario [2] aims for quite high core densities of ~3.5×10^{20} m^{-3}, so that the required SOL density is easily within reach for typical ratios of separatrix to line-averaged density of ~3. The Snowflake shows a modest reduction in the required density to ~6×10^{19} m^{-3}, with similar values for the stronger reduction, with low temperature being achieved at a density of ~2.5×10^{19} m^{-3}. The heat flux is substantially reduced in this configuration as well due to the larger wetted area, with acceptably low heat fluxes being achievable even for the lowest densities considered.

III. PARTICLE EXHAUST WITH COMPACT SYSTEMS

The conventional particle exhaust strategy in tokamaks such as ITER is to implement a highly shaped 'vertical target' divertor, which promotes high neutral gas pressures in the private flux region near the divertor strike points, conducive to efficient pumping [18]. However, as mentioned above, space is limited in FNSF designs for such optimized PFC structures, and so it is desirable to pump in a more simplified manner using pumping ducts located on the SOL side of the divertor

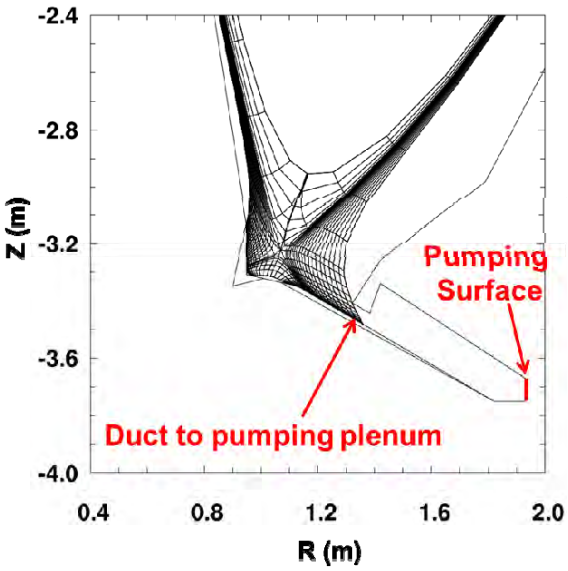

Fig. 4: Layout of the SOL-side pumping system

strike point (Figure 1). Since fluxes are reduced in this region compared to near-strike-point pumping enabled by a vertical target, it may be challenging to produce the needed pressures to ensure adequate particle removal.

The particle exhaust of the ST-FNSF has been examined using a semi-analytic model for the pumping developed for the DIII-D cryo-pumping systems [19,20] and extended as part of the design of a pumping system for the NSTX-U. This model requires that the divertor density, temperature, and particle flux profiles be known, and uses a first-flight neutral model to calculate the pressure in a candidate pumping volume. To provide the plasma profiles, the parallel heat flux profile is projected by assuming a SOL width as described above, and using MHD equilibria to map this to the divertor. Since the divertor temperature must be in the range 2-10 eV, we assume that T_e=5 eV. With these two quantities, we can then reconstruct the plasma density and particle flux profiles using standard Bohm boundary conditions on the sheath [21].

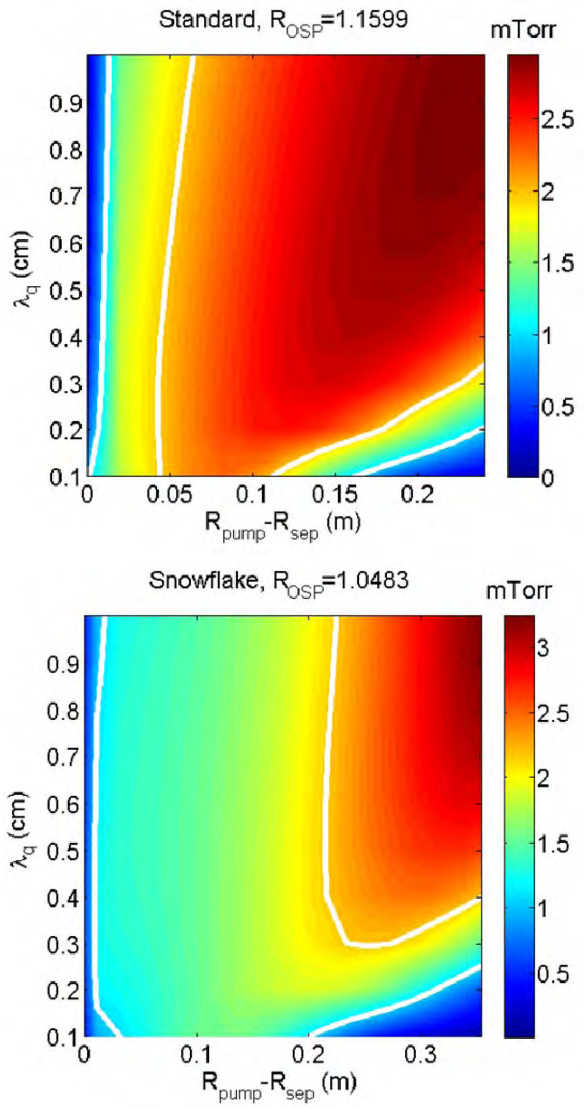

Fig. 5: Predicted plenum pressure vs. pump entrance position and SOL width for a) Standard and b) Snowflake configurations

The semi-analytic model also takes as input the geometry of the pumping volume, in particular the radial position, length, and height of the duct leading into the plenum (see Figure 4). These parameters have been optimized using the semi-analytic model, to produce a geometry that results in the highest plenum pressures. For example, figure 5 shows the plenum pressure as a function of the position of the duct entrance R_{pump} and SOL width λ_q, as calculated for the Standard and Snowflake configurations. In this calculation, the pumping speed is assumed to be 24 m^3/s for each pump, with one located in the upper and one in the lower divertor. This is a similar pumping speed to that achieved using cryogenic rings in DIII-D [18], although in ST-FNSF different technology may be required to provide exhaust in steady-state without the need for regeneration [22,23]. As Figure 5 shows, the optimal pump entrance location depends on the SOL width. Since this is uncertain at present, a pump position must be chosen that gives high performance over a broad range of SOL width assumptions. For both the Standard and Snowflake configurations, this indicates a pump entrance located at R_{pump}~1.3m as optimal.

While the particle throughput requirements of ST-FNSF are not yet well defined, we can estimate the minimum pumping needed as that which exhausts the particle input from neutral beam injection (NBI). The fueling and hence required pumping rate depends on the beam energy: with positive NBI at 120 keV, the required pressure is 2 mTorr at the assumed pumping speed, while if negative NBI at 500 keV is assumed a pressure of only 0.5 mTorr is needed. As Figure 5 shows, for a plenum entrance located at R=1.3m, pressures well above these levels are achievable over a wide range of SOL widths, indicating that this type of pumping configuration is indeed sufficient.

The density level that can be achieved by each of the pumping configurations has also been estimated. To accomplish this, the divertor temperature is varied such that the pumped flux matches the NBI input (in this case we only consider positive NBI, since the larger input in this case provides the more challenging exhaust requirement). The resulting divertor density, temperature, and heat flux are then used in a two-point model of the parallel plasma transport to yield the upstream density [21]. Finally it is assumed that the line-averaged to separatrix density ratio is 3, and the Greenwald fraction [24] is calculated as $f_G=\langle n_e\rangle \pi a^2/I_p$. As shown in Figure 6, both the Standard and Snowflake divertor configurations are able to pump the plasma down to f_G ~0.7-0.8, with similar levels attainable in the two configurations (due to the similar wetted areas). This is sufficient for the ST-FSNF scenario studied here, which optimizes to a density of f_G~0.8. If a lower density is required, or if higher particle input needs to be exhausted, the pumping speed of the system could be increased above what is assumed here.

As a final check on the pumping capabilities of these simple geometries, realistic pumping has been included in the SOLPS calculations. These calculations allow a model for the full radial T_e profile, as opposed to assuming a constant value as is

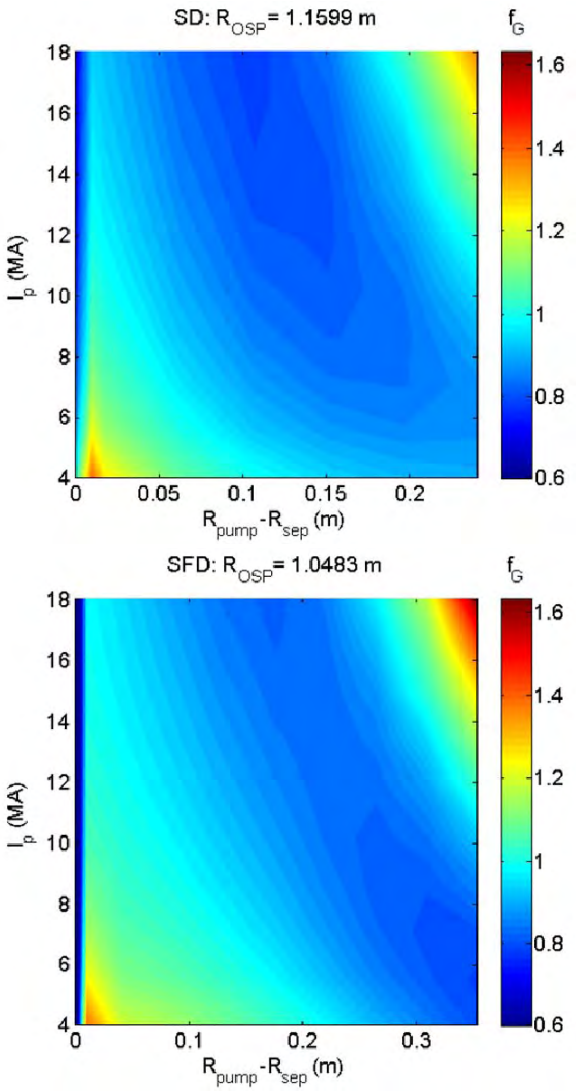

Fig. 6: Predicted Greenwald fraction vs. pump entrance and SOL width for a) Standard and b) Snowflake configurations, assuming positive NBI as the only particle input

done in the semi-analytic approach, and also include a much more comprehensive neutral transport model (which becomes important at the low T_e expected in the ST-FNSF divertor, where charge exchange collisions dominate). The plenum geometry in this modeling is based on the optimization using the semi-analytic model, with an entrance located at R=1.3 for both the Snowflake and Standard configurations. Pumping is performed on a surface at the end of the duct (Figure 4), with a particle recycling coefficient chosen to yield a pumping speed of 24 m^3/s. As before, density scans were performed for each case, in order to define the upstream density range that is consistent with attaining sufficiently high plenum pressure. In addition to these two divertor configurations, the Super-X case has also been modeled; in this case the radial extension of the leg naturally allows for PFR-side pumping without excessive shaping of the targets near the core plasma (see figure 1). As shown in Figure 7, all three configurations are again able to

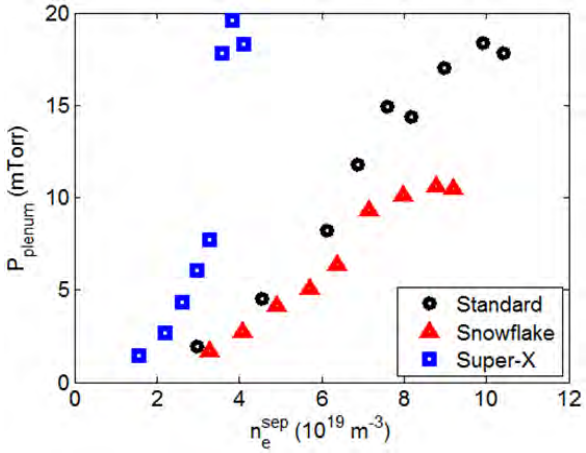

Fig. 7: SOLPS-calculated plenum pressure vs midplane density for the three divertor configurations

produce high pressures, in excess of 5 mTorr according to this better calculation. Again the Super-X shows better performance at lower upstream density, due to the lower T_e higher n_e divertor plasma produced in this configuration. For all three configurations, the pressures produced are far in excess of the needed 2 mTorr at the upstream densities that are consistent with power handling and low T_e. These calculations confirm that sufficient pumping (of the main ions, at least) can be achieved without complicated and space-consuming vertical target shapes and related baffling structures near the X-point. Further analysis is required to test the ability to pump helium ash in these configurations, which is necessary for the successful operation of an FNSF.

IV. Conclusions

The power and particle exhaust requirements of an ST-FNSF have been analyzed, using a combination of 0-D projections and 2-D modeling. For power exhaust, it is found that, for the SOL width considered a density range can be identified that produces a divertor plasma with temperature reduced below 10 eV as needed to minimize net erosion, and with heat fluxes reduced to ~5 MW/m^2, which is consistent with current technological capability. The density at which this is achieved depends on the divertor configuration, with lower density being adequate in the Snowflake and Super-X configurations; these configurations (especially the Super-X) may allow lower core density operation if needed to, e.g, ensure efficient current drive. However, in all cases the required density is well within the range anticipated for the ST-FNSF design point considered, which favors high core density operation. The heat fluxes in the Super-X are also considerably reduced, providing quite a bit of margin if the SOL width were to be significantly narrower than assumed here. Therefore, although a more conventional Standard divertor may indeed be adequate depending on the SOL width, a Super-X provides a conservative approach where adequately low temperatures and heat fluxes are relatively easily achievable.

The particle exhaust requirements appear to also be within reach, based on both semi-analytic projections and SOLPS modeling. Even with SOL-side pumping relatively far from the highest plasma fluxes, plenum pressures more than high enough to exhaust the particle input from positive NBI can be achieved for all divertor configurations considered. While this provides a basic test of feasibility, clearly for ST-FNSF helium exhaust will also need to be considered and will be the focus of future work.

REFERENCES

[1] Y.K.M. Peng et al, "Fusion Nuclear Science Facility (FNSF) before upgrade to Component Test Facility (CTF)", Fus. Sci. Tech. **60** (2011) 441.

[2] J. Menard et al, "Studies of ST-FNSF mission and performance dependence on device size", 1st IAEA DEMO Programme Workshop, Los Angeles, CA, USA, 15-18 Oct 2012.'

[3] V.A. Soukhanovskii et al, "Divertor heat flux mitigation in the National Spherical Torus Experiment", Physl. Plasmas **16** (2009) 022501.

[4] T.K. Gray, R. Maingi, V.A. Soukhanovskii, J.E. Surany, J.-W. Ahn, and A.G. McLean, "Dependence of divertor heat flux widths on heating power, flux expansion, and plasma current in NSTX", J. Nucl. Mat. **415** (2011) S360.

[5] M.A. Makowski et al, "Analysis of a multi-machine database on divertor heat fluxes", Phys. Plasmas **19** (2012) 056122.

[6] B. LaBombard et al, "Scaling of the power exhaust channel in Alcator C-Mod", Phys. Plasmas **18** (2011) 056104.

[7] T. Eich et al, "Inter-ELM power decay length for JET and ASDEX-Upgrade: measurement and comparison with heuristic drift-based model", Phys. Rev. Lett. **107** (2011) 215001.

[8] R.J. Goldston, "Heutistic drift-based model of the power scrape-off width on low-gas-puff H-mode tokamaks", Nucl. Fusion **52** (2012) 013009.

[9] K. Tobita et al, "Compact DEMO, SlimCS: design progress and issues", Nucl. Fusion **49** (2009) 075029.

[10] P.C. Stangeby and A.W. Leonard, "Obtaining reactor-relevant divertor conditions in tokamaks", Nucl. Fusion **51** (2011) 063001.

[11] R. Schneider et al, "Plasma edge physics with B2-EIRENE", Contrib. Plasma Phys. **46** (2006) 3.

[12] B.J. Braams, "Radiative divertor modelling for ITER and TPX", Contrib. Plasma Phys. **36** (1996) 276.

[13] D. Reiter, M. Baelmans, and P. Boerner, "The EIRENE and B2-EIRENE codes", Fus. Sci. Tech. **47** (2005) 172.

[14] Y.R. Martin, T. Takizuka, and ITPA CDBM H-mode threshold database working group, "Power requirements for accessing the H-mode in ITER", J. Phys.: Conf. Ser. **123** (2008) 012033.

[15] D.D. Ryutov, "Geometrical properties of a 'snowflake' divertor", Phys. Plasmas **14** (2007) 064502.

[16] P.M. Valanju, M. Kotschenreuther, S.M. Mahajan, and J. Canik, "Super-X divertors and high power density fusion devices", Phys. Plasmas **16** (2009) 056110.

[17] A.S. Kukushkin et al, "Scaling laws for edge plasma parameters in ITER from two-dimensional edge modelling", Nucl. Fusion **43** (2003) 716.

[18] A.S. Kukushkin et al, "Basic divertor operation in ITER-FEAT", Nucl. Fusion **42** (2002) 187.

[19] R. Maingi, J.G. Watkins, M.A. Mahdavi, and L.W. Owen, "Pump plenum pressure dependence on divertor plasma parameters and magnetic geometry in the DIII-D tokamak", Nucl. Fusion **39** (1999) 1187.

[20] R. Maingi, J.G. Watkins, M.A. Mahdavi, and R.J. Colchin, "Neutral pressure dynamics in the upper plenums in the DIII-D tokamaks", Nucl. Fusion **44** (2004) 909.

[21] PC Stangeby, "The plasma boundary of magnetic fusion devices", Institute of Physics, 2000.

[22] K. Ioki et al, "Ceramic turbomolecular pum,ping system in reactor structure of FER", Fus. Eng. Design **10** (1989) 223.

[23] C.A. Foster, D.E. Schechter, R. Scott Willms, David Dogruel, and Larry Baylor, "A continuous cryogenic diffusion pump for fusion reactors", 21st Symposium on Fusion Engineering, Knoxville, TN, 2005.

[24] M. Greenwald et al, "A new look at density limits in tokamaks", Nucl. Fusion **28** (1988) 2199.